UV-Ozone Cleaning of Supported Poly(vinyl pyrrolidone)-Stabilized Palladium Nanocubes: The Effect of Stabilizer Removal on Morphology and Catalytic Behavior

Micaela Crespo-Quesada,[†] *Jean-Michel Andanson,*[†] *Artur Yarulin,*[†] *Byungkwong Lim,*[‡]

Younan Xia[‡] *and Lioubov Kiwi-Minsker*[†,*]

[†]Group of Catalytic Reaction Engineering, Ecole Polytechnique Fédérale de Lausanne, 1015 Lausanne, Switzerland

[‡]Department of Biomedical Engineering, Washington University, Saint Louis, Missouri 63130, United States

RECEIVED DATE

AUTHOR INFORMATION

[*]*Corresponding author: EPFL-SB-ISIC-GGRC, Station 6;* lioubov.kiwi-minsker@epfl.ch; 0041 21 693 3182; 0041 21 693 3667.

ABSTRACT

Poly(vinyl pyrrolidone) (PVP)-stabilized Pd nanocubes were synthesized, deposited on a carbon-based support and subsequently treated with UV-Ozone (UVO) in order to eliminate the traces of PVP still present on the surface. Cubes, being a thermodynamically unfavorable shape, are very prone to restructuring to minimize the interfacial free energy, and thus allow the assessment of their morphological stability during UVO cleaning. The process of PVP removal was monitored by X-ray photoelectron spectroscopy (XPS), X-ray diffraction (XRD) and *in-situ* attenuated total reflection infrared spectroscopy (ATR-IR). High-resolution scanning electron microscopy (SEM) imaging was used to evaluate the morphology of the nanocubes. The effect of PVP removal was also studied in the hydrogenation of acetylene, showing a fourfold increase of activity. This method can be applied to nanoparticles of other common shapes, which expose different crystal planes, in order to study the structure sensitivity of chemical reactions.

INTRODUCTION

Structure sensitivity is of great interest in heterogeneous catalysis. Structure sensitive reactions, such as Suzuki,[1] Heck,[2] and hydrogenation reactions[3] are strongly affected by the variation in the morphology of the active nanoparticles (NPs) due to well-known electronic and geometric effects.[3-5] The ratio of surface atom types (vertex, edge, and face) changes substantially with NP size. The fraction of face atoms located on (111) and/or (100) crystal planes increases with size at the expense of both edge and vertex atoms.[3,6] This change results in a *size effect* which manifests itself with an increase (antipathetic structure-sensitivity) or decrease (sympathetic structure-sensitivity) of TOF with particle size.[7] Furthermore, a variation in shape also implies important morphological differences: cubes only present (100) face atoms, octahedra present only (111) face atoms and cube-octahedra (near-spheres) a mixture of both.[3,6] This induces a *shape effect*, especially if each type of surface atom possesses a different reactivity. Therefore, such shape and size effects could be used in structure-sensitive reactions for *optimizing* the catalyst.

The study of the reactivity of different crystal planes has been carried out theoretically,[8-10] as well as on 2D model catalysts ranging from single crystals[11] to monodispersed nanoclusters deposited by lithography techniques.[12] The study on shape-controlled nanoparticles is another alternative. The challenging task of shape-controlled synthesis of NPs has attracted significant attention over the past years.[13-14] Colloidal techniques allow the formation of monodispersed NPs with desired sizes and shapes.[13] With these techniques, when the reduction of the metal is slow enough, specific surface capping agents can guide the growth of thermodynamically unstable shapes by preferential growth on the least strongly capped crystal plane.[14-15] In order to study the true catalytic behavior of each crystal plane, this approach requires the removal of the stabilizer and/or capping agents used during synthesis. Such compounds are commonly found on the surface of the NPs in trace amounts in spite of the extensive cleaning procedures to which they are subjected.[16-17]

In order to remove these substances, plasma cleaning,[18] calcination,[19] heat [20-21] and high temperature

hydrogen treatments[22] have been reported in the literature. These techniques, however, either require special equipment, or can compromise the morphological integrity of the nanoparticles due to harsh treatment conditions. UV-ozone (UVO) is a useful alternative capable of yielding nearly atomically-clean surfaces.[23] Indeed, this technique has been used in the elimination of various organic capping agents from colloidal Pt[24] and Au[25] nanoparticles. It is based on the combination of short wavelength UV light and ozone at room temperature.[23]

In this work, poly(vinyl pyrrolidone) (PVP)-stabilized Pd nanocubes were synthesized, deposited onto a carbon-based support and treated with UVO. Cubes, being a thermodynamically unfavorable shape, are prone to restructuring in order to minimize the interfacial free energy. This allowed assessing their morphological stability during UVO cleaning. The extent of PVP depletion was studied *ex-situ* via surface characterization with X-ray photoelectron spectroscopy (XPS) and X-Ray diffraction (XRD) and *in-situ* via attenuated total reflection infrared spectroscopy (ATR-IR). IR spectroscopy has been proven to be a very useful tool to study molecular interactions of complex systems as well as kinetic phenomena.[26] ATR-IR spectroscopy is particularly suitable for the investigation of solid/fluid interfaces as it is possible to probe only molecules located in the first (few) micrometer(s) over the surface of an Internal Reflection Element.[27] The catalysts were also tested in the gas-phase hydrogenation of acetylene in order to elucidate the effect of the stabilizing agent on the catalytic response.

To the best of our knowledge, this is the first time that this method is applied for cleaning supported nanoparticles aiming at preparing shape-tailored PVP-free Pd-NP catalysts which could provide valuable information on the structure-sensitivity of chemical reactions.

EXPERIMENTAL SECTION

Chemicals and materials. Poly(vinyl pyrrolidone) (PVP, MW≈55,000, Aldrich), citric acid (Fisher), sodium tetrachloropalladate (II) (Na_2PdCl_4, Aldrich), and potassium bromide (KBr, Fisher) were all used as received without further purification. Acetylene was purchased from Carbagas and hydrogen

was produced on site with a hydrogen generator NMH_2 500 (Schmidlin-DBS AG).

Catalyst preparation. The synthetic route for shape-tailored Pd nanocubes can be found in detail elsewhere.[16] In a typical synthesis, PVP and KBr (capping agent) were dissolved in bidistilled water in a 25 mL round-bottom flask equipped with a teflon-coated magnetic stir bar and a reflux condenser and heated up to the target temperature. Na_2PdCl_4 was dissolved in bidistilled water at room temperature, and this aqueous solution was then rapidly added to the flask. The molar ratio of Pd to the repeating unit of PVP was kept at 1:5. The reaction mixture was kept at the target temperature for 3 h and then the product was collected by flocculation with acetone, and finally washed twice with ethanol to remove excess PVP and KBr.

Commercially available Inconel sintered metal fibers filters ($SMF_{Inconel}$, Bakaert Fibre Technology, Zwegem, Belgium) were used as a growth-media for carbon nano fibers (CNF). Before any use, the filters were calcined at 650 °C for 3 h in order to increase the roughness of the fiber surface and create the surface sites for CNF growth. The SMF panels were subsequently cut in round disks of 24 mm in diameter. The method of preparation of carbon nanofibers over Inconel sintered fiber filters ($CNF/SMF_{Inconel}$) is described elsewhere.[28] Briefly, carbon nanofibers were grown on SMF filters by the catalytic pyrolysis (chemical vapor deposition, CVD) of ethane in the presence of hydrogen. The synthesis was carried out in a tubular quartz reactor with 24 mm internal diameter posed in a tubular oven. The SMF filters were first reduced in hydrogen (120 Nml/min). The temperature was increased 10°C/min and held at 625°C for 2h. Then, the reactor was heated up 675°C, and a mixture $Ar:C_2H_6:H_2$ = 80:3:17 (flow 600 ml (STP)/min) was introduced for 1h.

Palladium nanoparticles were deposited onto $CNF/SMF_{Inconel}$ support by incipient wetness impregnation. This method implies deposition of nanoparticles by plunging the support directly into the solution with metal nanoparticles. The discs were subsequently dried under vacuum at 50°C overnight. The metal loading can be adjusted by using multiple impregnation steps.

UV-ozone cleaning was used in order to eliminate traces of PVP from the surface of the nanoparticles.

The method uses UV light that includes wavelengths of 185 and 257 nm, where the former generates ozone upon interacting with molecular oxygen and the latter excites the organic contaminating molecules.[23] The irradiation with the UV light was conducted using a Helios Quartz (Milan, Italy) 8 W low-pressure mercury lamp emitting at 185 and 257 nm inside a custom-made metallic enclosure. The sample was placed at 5 mm from the lamp during a given amount of time and was then removed from the UVO chamber.

Characterization. To determine the amount of Pd deposed, the catalyst was dissolved in aqua regia and the sample was analyzed by atomic absorption spectroscopy (AAS) with a Shimadzu AA-6650 spectrometer and an air-acetylene flame. The specific wavelength used for Pd^{2+} was 475 nm.

X-ray photoelectron spectroscopy (XPS) data were collected by an Axis Ultra instrument (Kratos analytical, Manchester, UK) under ultra-high vacuum condition ($<10^{-8}$ Torr) and using a monochromatic Al Kα X-ray source (1486.6 eV). The adventitious carbon 1s peak was calibrated at 284.5 eV and used as an internal standard to compensate for any charging effects.

Powder X-ray diffractograms (XRD) were recorded on a Bruker/Siemens D500 incident X-ray diffractometer using Cu Ka radiation. The samples were scanned at a rate of 0.02º $step^{-1}$ over the range $30º \leq 2\theta \leq 90º$ (scan time = 5 s $step^{-1}$). Diffractograms were identified using the JCPDS-ICDD reference standard for Pd (46-1043).

In order to perform the infrared spectroscopy experiments, a homemade ATR high-pressure stainless steel (316 L) cell was equipped with an internal reflection element made of Ge crystal (angle of incidence 60°; 6 active reflections). A PTFE ring was used as sealing between the multiple reflection crystal and the cell to avoid leaks. Before starting the measurements, the crystal was polished using diamond paste to remove any contaminant traces from previous experiments. During the experiments, the temperature of the cell was kept constant at 293K. Circa 500 μl of a colloidal solution containing the nanoparticles in ethanol was cast-dropped on the top of the crystal. The ATR cell was either closed in order to flow N_2, H_2 or CO gas, or the UV lamp was placed 5 mm over the crystal, allowing the in-situ

monitoring of the UVO cleaning process. Spectra were recorded using an EQUINOX-55 Fourier transform infrared spectrometer (Bruker Optics) purged continuously with dried air. IR spectra were recorded on the range of 4000–600 cm^{-1} with a resolution of 2 cm^{-1} using a liquid N_2-cooled mercury cadmium telluride (MCT) detector. More details about the ATR cell and ATR-IR spectroscopy in the field of catalysis can be found in a recent review.[27]

The morphology of the catalyst surface was studied by scanning electron microscopy (SEM) with a FEI XL30 SFEG microscope equipped with a TLD detector. The acceleration voltage was varied between 10 and 20 kV and the working distance was kept between 4 and 6 mm. Transmission Electron Microscopy (TEM) was used to study size and structure of unsupported Pd nanoparticles. The microscope used was a CM20 FEG (Philips) operated at 200kV. High-resolution (HRTEM) images were recorded with a CM300 FEG (Philips/FEI) microscope operated at 300 kV. The solution containing Pd nanocubes was cast dropped on Cu grids and dried in air under infrared light for at least an hour before introducing them into the microscope.

Catalytic testing. The hydrogenation of acetylene was carried out in a jacketed tubular reactor with an internal diameter of 12 mm. The catalyst was placed in the reactor between two metallic rings to ensure that the position of catalyst was perpendicular to that of the gas flow. A fixed bed of glass beads inside the reactor was used to homogenize and preheat the flow of reactants upstream of the catalyst. During the reaction, the pressure was maintained at 1.04 bar. Products were monitored on-line by gas chromatography (HP 6890, Agilent Technology AG, Switzerland) using a Carboxen 1010 (Supelco, Fluka Holding AG, Switzerland) capillary column. Samples were taken every 10 min on-stream.

RESULTS AND DISCUSSION

Preparation and characterization of the catalysts. Figure 1 shows typical TEM and HRTEM images of Pd nanocubes. The inset in Figure 1A gives a schematic illustration of a face-centered cubic (*fcc*) lattice, where atoms belonging to (100) crystal planes, corners, and edges are evidenced. By

counting over 200 nanoparticles from different regions of the sample, a mean particle size of 10.1 ± 0.9 nm and a yield of over 95% for the cubic shape enclosed by (100) facets were estimated. The nanocubes were subsequently immobilized by incipient wetness impregnation on supports of carbon nanofibers grown on sintered metal fibers ($CNF/SMF_{Inconel}$). The loading of Pd could be conveniently varied by altering the concentration of the colloidal suspension and/or by changing the number of impregnations.

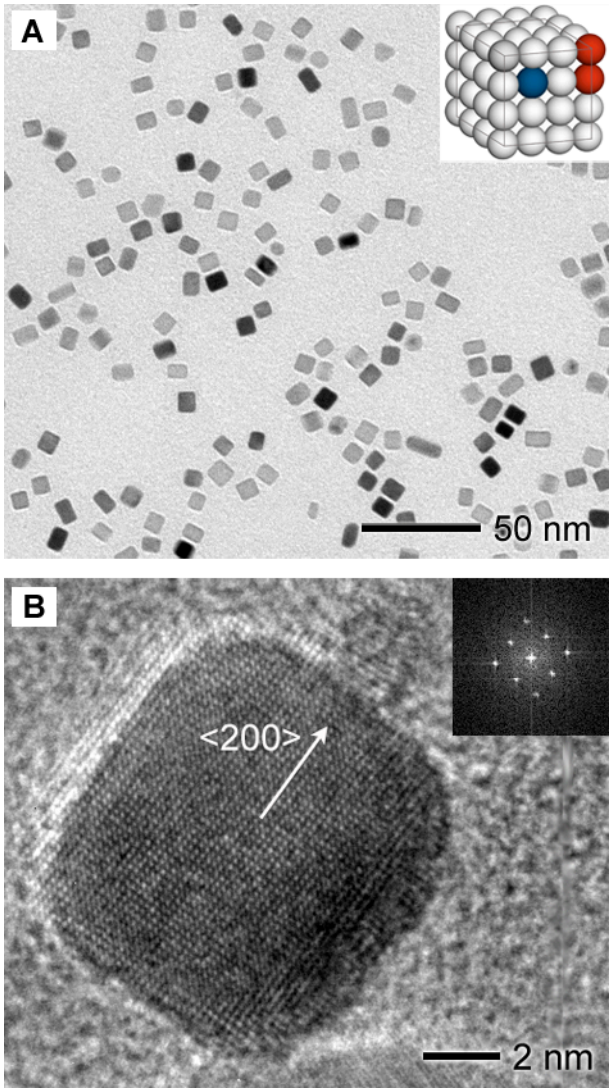

Figure 1. (A) TEM image of the Pd nanocubes: The inset is a schematic representation of an fcc nanocube, where the Pd100 face atoms as well as the corner and edge atoms are evidenced; (B) High-resolution image and FT pattern (inset) of a single nanocube. The lattice spacing of 1.94 Å can be indexed to the {200} reflection of Pd.

Figure 2 shows SEM images of samples involved in different stages of the preparation procedure.

Figure 2A shows an image of the individual fibers of approximately 8 μm in diameter of the raw $SMF_{Inconel}$ after calcination. After reduction and one hour of CVD, a thick and uniform layer of CNF was formed on the $SMF_{Inconel}$, as seen in Figure 2B. An increase in magnification (Figure 2C) shows some interesting features of this material: the intertwined, yet open structure of CNF can be observed in addition to the Ni/Fe nanoparticles of approximately 100 nm in size that served as a catalyst for the formation of CNF. The smaller, bright squares are the 10-nm Pd nanocubes, already visible at relatively low magnifications (x50,000). It can be appreciated that the dispersion of the Pd nanoparticles was uniform and that no agglomerates were formed during the impregnation and drying steps. Furthermore, probably due to the presence of PVP on their surfaces, the nanocubes tended to deposit on the outermost layers of CNFs, leaving the fibers deep inside free of Pd nanocubes. Finally, Figure 2D shows a high-magnification SEM image, where the shape of the nanoparticles can be clearly resolved. XPS analyses of the as-prepared catalyst revealed the presence of nitrogen due to PVP (N/Pd atomic ratio of roughly 1) as well as the absence of Br-.

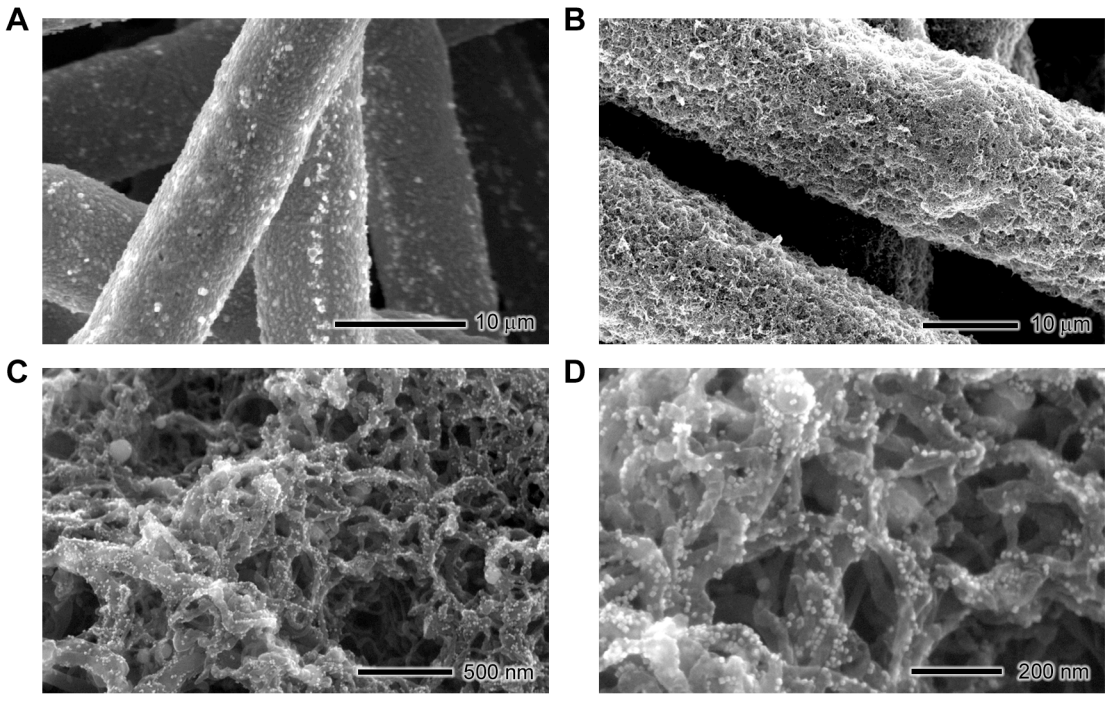

Figure 2. High resolution SEM images depicting the catalyst's preparation procedure. (A) Calcined $SMF_{Inconel}$, (B) CNF grown on SMF after ethane CVD, (C) Close-up image of the CNF network and (D)

High magnification image of the supported nanocubes.

Removal of PVP. Thermal treatments at relatively high temperatures (~573 K) have been employed to eliminate organic capping agents without significantly altering the shape and size of metallic nanoparticles.[20-22,29] In this work, the as-prepared catalyst was also subjected to a cyclic oxidation/reduction treatment, which was proven to eliminate the carbonaceous deposits formed during the combustion of organic molecules.[22] The catalyst was exposed to 2% O_2/N_2 at 393 K for 1 h, after which the gas was switched to 2% H_2/Ar and kept at the same temperature for one additional hour. The cycle was then repeated. Despite that the treatment eliminated PVP from the catalyst (as revealed by XPS), the shape, size, and distribution were drastically altered as seen by SEM imaging (Figure S1, Supporting Information).

Since the aim of this work was to eliminate PVP while keeping the morphology of the active phase intact, the high-temperature treatment method was deemed not applicable, and UVO cleaning was thus tested. The available evidence indicates that UVO cleaning is primarily the result of photosensitized oxidation processes. The contaminant molecules are excited and/or dissociated due to the absorption of short wavelength UV light. Simultaneously, atomic oxygen and ozone are produced when O_2 is dissociated due to the absorption of UV with wavelengths shorter than 245.4 nm. Atomic oxygen is also produced when ozone is dissociated through the absorption of both the UV light and radiation at longer wavelengths. The excited contaminant molecules and the free radicals produced by the dissociation of contaminant molecules, react with atomic oxygen to form simpler volatile molecules.[23]

High-resolution SEM imaging is known to be a very useful technique in the assessment of morphological changes of nanoscale, shape-tailored Pd nanoparticles during PVP removal. It was found that the shape, size, and distribution of the nanoparticles were well maintained even after 6 hours of UVO treatment, as shown in Figure 3 confirming that UVO cleaning was suitable for this application. It is however worth noting that a certain degree of nanoparticle reassembly was expected, as reported previously in the literature.[24,29]

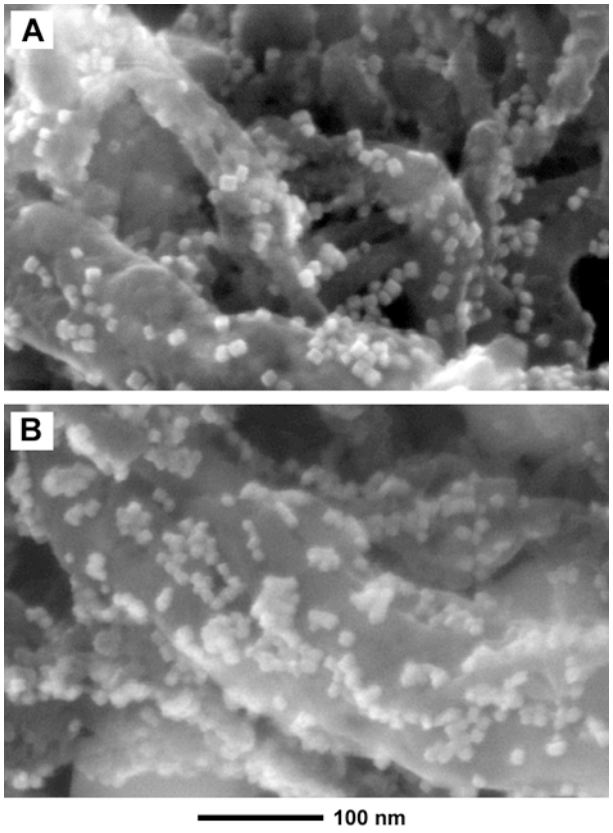

Figure 3. High magnification SEM pictures (A) before and (B) after 6h of UVO treatment.

The elimination of PVP via UVO treatment was further analyzed *ex situ* by XPS and XRD and *in-situ* via ATR-IR spectroscopy. Figure 4A shows the XPS survey spectra of the fresh catalyst, as well as after 2, 4 and 6 hours of UVO treatment, respectively. In this case, the N 1*s* peak (400 eV), while visible in the fresh catalyst, was drastically reduced after only 2 hours of treatment. High-resolution scans of the zone revealed that 63% of the N present in the fresh catalyst was eliminated during the first 2 hours of treatment. Furthermore, the amount of N was undetectable after 4 and 6 hours of treatment. It was found, however, that the UVO cleaning procedure was not able to eliminate PVP from the side which was facing opposite to the lamp. Figure 4B shows the XPS spectra for both sides of the catalyst after 4 hours under UVO treatment where the peak corresponding to N can be distinctively seen on the side facing away from the lamp.

It can be appreciated from Figure 4B that the peaks corresponding to Pd widen throughout the cleaning process. High-resolution scans reveal thatthe amount of $Pd^{\delta}+$ on the surface of the catalyst

increased remarkably by the end of the treatment. Indeed, the amount of $Pd^{\delta}+$ increases from 12% in the fresh catalyst to 54% after 4 hours of treatment. However, this increase is probably due to the passivation of Pd through dissociative chemisorption of oxygen and not to the formation of bulk PdO. Studies on the growth mechanism of PdO nanoparticles showed that the morphology of the nanoparticles was unaltered under 1 bar of O_2 at relatively high temperatures.[30] $Pd_{(100)}$ and $Pd_{(111)}$ were found to form a simple (2x2) oxygen overlayer when exposed to molecular oxygen at room temperature.[31] Furthermore, the absence of morphological changes on the nanoparticles after treatment (Figure 3) suggest that no bulk PdO was formed, since it is known that due to high lattice parameter differences, its growth induces cracking and disintegration of the metallic surface.[30,32]

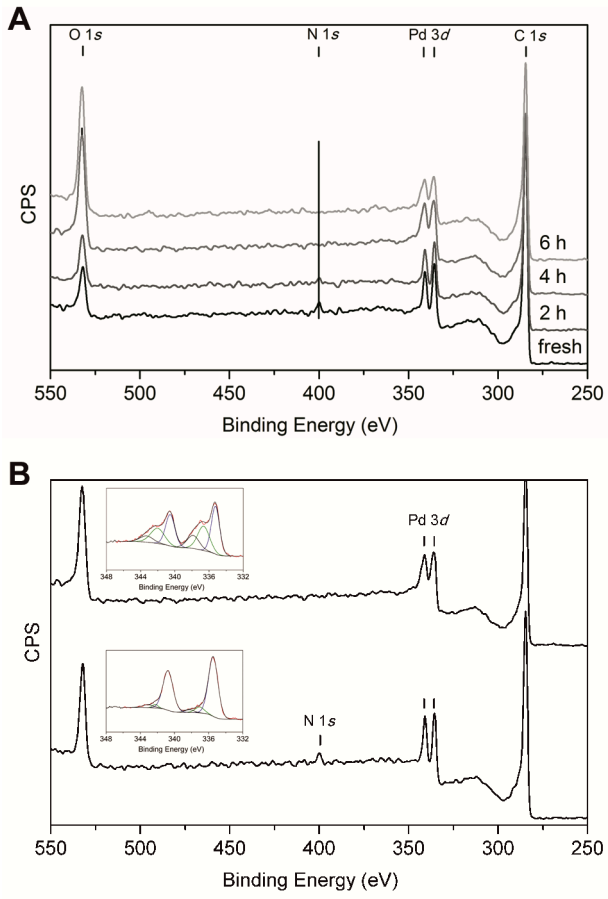

Figure 4. (A) General XPS survey scans of the fresh catalyst as well as after 2, 4 and 6h of UVO treatment; (B) General XPS survey scans of the supported nanocubes after 4h of UVO treatment of the side facing away from the UVO lamp (bottom trace) and facing towards the UVO lamp (top trace). The

insets correspond to high-resolution scans of the Pd $3d_{5/2}$ region.

In order to verify this hypothesis, XRD coupled with XPS measurements were performed on Pd black powder both in its fresh state and after 6 hours of UVO treatment. Pd black was chosen over the nanocubes due to the weak XRD signals obtained with the latter. XRD measurements showed the exclusive presence of metallic Pd on both fresh and treated samples (see Figure S2, Supporting information), whereas XPS detected an increase of 20% in the amount of Pd^{δ}+ thus confirming the passivating effect of UVO treatment. The catalyst was finally treated in hydrogen at 393 K for half an hour and the relative amounts of Pd(0)/Pd^{δ}+ were found to reverse to those found in the fresh catalyst.

It is also important to study the effect of the UVO treatment on the CNF, since it might change the surface chemistry of the latter. The nature of the oxygen groups present on the surface of the CNF can be studied with XPS. Carbon atoms differ in their binding energy if they're bonded to an oxygen atom (phenols, ethers, carbonyl groups) or to two oxygen atoms (carboxyl and lactone groups).[33] Their corresponding signals appear as satellites on the high binding energy side of the main C1*s* peak, as shown in Figure S3. The C1*s* spectra can be resolved into six individual component peaks representing carbidic carbon (Peak I), graphitic carbon (Peak II), phenol or ether groups (Peak III), carbonyl groups (Peak IV), carboxyl or ester groups (Peak V) and shake-up satellite peaks due to π-π* transitions in aromatic rings (Peak VI).[34-35] It can be seen that there's already a significant amount of oxygen-coordinated carbon in the as-prepared support (Figure S3A), although the vast majority correspond to phenol, ether and carbonyl groups, which are weakly acidic to neutral in nature. A common way of decreasing the hydrophobicity of as-prepared CNF is by deliberately adding oxygenated surface groups by treating them in boiling hydrogen peroxide (Figure S3B). Following activation, the amount of graphitic carbon diminishes sensibly, mainly in favor of carboxylic groups, which are strongly acidic. It can be seen that a 4h treatment under UVO (Figure S3C) also increases the relative amount of carboxylic groups on the surface of CNF. Furthermore, the O/C ratio was found to be an order of

magnitude lower in as-prepared CNF as compared to activated/UVO-treated CNF, suggesting that the absolute amount of oxygen-containing groups is significantly increased by the treatment. Finally, the deposition of PVP-stabilized Pd nanoparticles (Figure S3D) does not seem to affect the relative amount of the different functionalities. It can be thus concluded that UVO-treatment increases the acidity of CNF.

The kinetics of PVP removal by UVO cleaning was followed by *in-situ* ATR-IR spectroscopy. The details of PVP IR bands assignment in a similar system (PVP on Pt) can be found elsewhere.[36] The evolution of the IR spectra during the first 30 minutes of treatment in the range of the C-H stretching and fingerprint region are given in Figure 5A and B, respectively.

A fast and homogeneous decrease of the concentration of the molecules involving the C-H stretching vibration (Figure 5A), as well as most of the PVP vibrations (Figure 5B), was observed. The decrease in the IR signal results from the elimination of PVP, the two most noticeable exceptions being the rising IR signal between 1850 and 1950 cm-1 and the change in the shape of the carbonyl stretching band in the range of 1600-1800 cm-1 during the first 5 minutes of UVO treatment. The C=O stretch of PVP is especially sensitive to the molecular environment, and the shift could indicate a change in the structure of PVP itself, in the interaction between the metal nanoparticle and PVP or in the hydrogen-bond network.

The rising signal at around 1900 cm-1 probably corresponds to carbon monoxide, a product of the decomposition of the PVP by UVO[23] that is known to have a high affinity for Pd.[37] Furthermore, Borodko *et al*. also found CO absorbed on Pt while studying the thermal decomposition of PVP on Pt.[36] In order to validate the assignment of the band to CO adsorbed on Pd, ATR-IR spectra of PVP/Pd and Pd nanoparticles (after UVO treatment) are shown on Figure 5C. After 3 hours of UVO treatment, PVP was removed and only a few bands (1900 and 1650 cm-1) are still visible. The broad signal rising at 1650 cm-1 typically corresponds to the water bending mode. The addition of CO over Pd leads to two positives bands at 1930 and 2045 cm-1 preceded by two negative signals at higher wavenumbers. The

presence of negative bands is an anomalous effect which is well known in IR spectroscopy for such thin and irregular metallic samples.[38] A similar experiment of CO on Pd particles before UVO treatment also confirmed the two CO absorption modes on Pd/PVP nanocubes. The two signals correspond to CO molecules adsorbed onto Pd in a linear (on-top) and bridged configuration at 2045 and 1930 cm-1, respectively, in accordance with the literature available on CO absorption on Pd stabilized by PVP.[39] The shift between the CO signal at 1900 cm-1 after UVO treatment, and the signal at 1930 cm-1 can be explained by the increase of the concentration of CO adsorbed on the surface of Pd.[37]

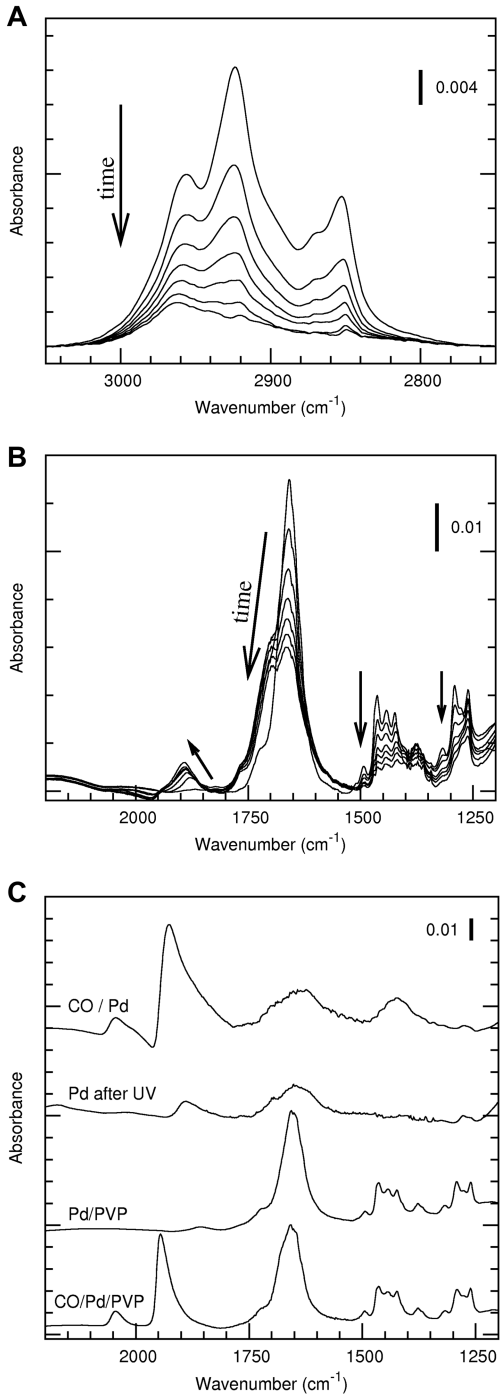

Figure 5. (A) and (B) ATR-IR spectra of PVP/Pd nanocubes under UVO treatment at 0, 5, 10, 15, 20, 25 and 30 minutes; (C) ATR-IR spectra of Pd nanocubes before and after UVO treatment (3 hours) under N_2 or CO atmosphere (Spectra have been offset for clarity reasons).

Acetylene hydrogenation. It is known that the reaction conditions during the stabilization of the catalyst may have a large effect on the composition and morphology of the carbonaceous layer on Pd

and on the kinetic properties of the catalyst under steady state.[3,40-42] The nature of the support could thus influence the catalytic behavior when its surface chemistry is modified.[43] The change in support acidity was studied with the preparation of a third catalyst (catalyst C). In this case, the support was pre-treated for 4 h under UVO and the PVP-stabilized Pd nanocubes were subsequently deposed on it. Table 1 summarizes the preparation procedure for the catalysts tested in the hydrogenation of acetylene and the Turnover Frequencies (TOF) obtained under the same experimental conditions at acetylene conversion of 25%. In separate experiments the kinetic regime has been confirmed.

TOF increased fourfold in the absence of PVP (catalysts A and B), suggesting that the stabilizing agent partially blocked the active sites of the nanoparticles as seen in Table 1. This trend had already been observed in the hydrogenation of ethylene over NPs stabilized by tetradecyltrimethylammonium bromide (TTAB) and PVP and it could be attributed to a weaker interaction of TTAB with metal surfaces.[44] Nevertheless, PVP-stabilized Pd nanocubes were found to be twice as active when supported on UVO-treated CNF/SMF supports. This result suggests that the increase in activity observed in catalyst B was probably partially due to the modification of the support during UVO treatment.

As seen in Table 1, selectivity was not significantly influenced by the treatment. Nonetheless, considering the experimental error, green oil formation was found to be favored in the UVO-treated samples (catalysts A and B), despite the fact that CO is formed and adsorbs on palladium during the decomposition of PVP, as seen by *in-situ* IR measurements. It is nonetheless worth noting that although carbon monoxide is frequently used to increase the selectivity towards ethyne,[40] the amount adsorbed is clearly far from saturation as it can be seen in Figure 5. Furthermore, CO was found to desorb from Pd much faster in the presence of acetylene.[45-47] Then, this effect probably arises from the change in support acidity after UVO. Indeed, increased support acidity was found to reduce the yield of olefin in the hydrogenation of acetylene,[48] propyne,[49] and 1,3-butadiene.[50]

Whereas the non-treated catalyst (A) was fairly stable, with a decrease of only 5% of the initial activity after 3.5 h on stream, catalysts B and C deactivated much more quickly, although the catalyst

that deactivated the most (15.5% of initial activity in 3.5 h) was the UVO-treated (catalyst B). There seems to be a correlation between support acidity and deactivation, as already reported in the literature.[49] This deactivation probably arises from a slight increase in the formation of green oil in catalysts B and C resulting from the increased acidity of the support. In all cases the behaviour of the PVP-stabilized nanocubes on UVO-treated CNF (catalyst C) was intermediate to that of the PVP-stabilized nanocubes (catalyst A) and the UVO-treated nanocubes (catalyst B).

A frequent problem encountered when working with shape-tailored nanoparticles is their morphological instability, especially when the reaction is carried out in colloidal solution[1,51-52] due to the strong dependence of interfacial free energy density on temperature and on the presence of adsorbed molecule on the surface of a nanocrystal.[53] However, the support seemed to grant high morphological stability to the nanocubes, which retained their shape and distribution even after 10 hours on stream (Figure 6).

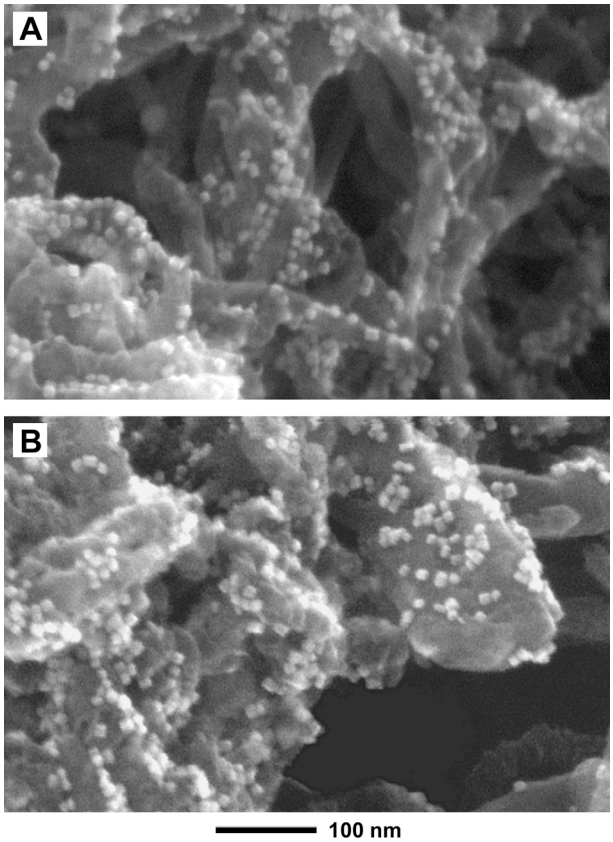

Figure 6. SEM images of the (A) fresh supported nanocubes and (B) after 10h on stream. Reaction

conditions: 393 K, C_2H_2:H_2:Ar = 1.2:20:78.8, 25% conversion.

CONCLUSIONS

PVP-stabilized Pd nanocubes, a thermodynamically unfavorable shape, were synthesized, deposited on CNF/SMF supports and treated with UVO in order to eliminate the trace amount of stabilizing agent still present on its surface. *Ex-situ* XPS analyses showed that N from PVP was already undetectable after 4h under UVO cleaning. The surface of the Pd nanocubes was found to passivate after the UVO treatment, but no bulk PdO phase was formed. Futhermore, the treatment was found to increase the number of oxygen-containing groups present on the surface of the CNF/SMF support, thus changing its acid/base properties. *In-situ* ATR-IR analysis showed that there was a homogeneous decrease of most PVP vibrations. CO was found to be generated from the decomposition of PVP and to adsorb on the surface of Pd although the coverage was far from saturation. High-resolution SEM imaging showed a remarkable morphological stability of the nanaocubes even after 6h of UVO treatment.

The catalyst was tested in the hydrogenation of acetylene. The removal of PVP increased the activity of the catalyst fourfold and selectivity towards green oil was found to increase after UVO treatment. The nanocubes were found to be morphologically stable under the reaction conditions used.

The method described herein can be thus used for treating supported nanoparticles of other common fcc shapes (octahedra, tetrahedra, cube-octahedra), which expose different types of crystal planes, in order to study the structure sensitivity of a particular chemical reaction under real operation conditions. This work is currently ongoing and the results will be published elsewhere.

ACKNOWLEDGMENT

The financial support of the Swiss National Science Foundation (Grant n° 200021-118067) is highly appreciated. The authors would also like to thank Pietro Tanasini (EPFL-SB-ISIC-GGEC) for the SEM images, Marco Cantoni (EPFL-SB-CIME) for the high-resolution TEM images, Nicolas Xanthopoulos (EPFL-SB-CIME) for the XPS measurements and Professor Alfons Baiker (ETH Zürich, Department of Chemistry and Applied Biosciences) for the use of his IR spectroscopy facilities. The Pd nanocube synthesis was supported by the National Science Foundation (DMR-0804088, to Y.X.).

ASSOCIATED CONTENT

Supporting information available: Experimental procedures; the effect of the catalyst calcination to remove PVP on the morphology of the nanocubes; XRD measurements showing the absence of bulk palladium oxides after UVO treatment and the effect of UVO on the chemistry of the support.

This information is available free of charge via the Internet at http://pubs.acs.org.

TABLES

Table 1. Summary of the catalysts used in this study and catalytic results[b]

Catalyst	% Pd[a]	CNF oxidized	PVP removed	TOF [s^{-1}]	S_{C2H4} [%]	Deactivation [%][c]
A	0.48	No	No	94.7±2.5	85.1±4.3	5.0
B	0.10	Yes	Yes	359.9±9.1	70.2±3.2	15.5
C	0.48	Yes	No	188.8±4.8	78.3±3.8	12.9

[a] Percentage expressed with respect to the amount of CNF.

[b] Reaction conditions: 393 K, C_2H_2:H_2:Ar = 1.2:20:78.8, 25% conversion.

[c] Expressed as percentage of initial activity lost in 3.5h on stream.

REFERENCES

(1) Narayanan, R.; El-Sayed, M. A. *J. Phys. Chem. B* **2005**, *109*, 12663.

(2) Le Bars, J.; Specht, U.; Bradley, J. S.; Blackmond, D. G. *Langmuir* **1999**, *15*, 7621.

(3) Molnar, A.; Sarkany, A.; Varga, M. *J. Mol. Catal. A* **2001**, *173*, 185.

(4) Teranishi, T.; Miyake, M. *Chem. Mater.* **1998**, *10*, 594.

(5) Coq, B.; Figueras, F. *J. Mol. Catal. A* **2001**, *173*, 117.

(6) Van Hardeveld, R.; Hartog, F. *Surf. Sci.* **1969**, *15*, 189.

(7) Che, M.; Bennett, C. O.; D.D. Eley, H. P. a. P. B. W. In *Adv. Catal.*; Academic Press: 1989; Vol. Volume 36, p 55.

(8) Kizilkaya, A. C.; Gracia, J. M.; Niemantsverdriet, J. W. *J. Phys. Chem. C* **2010**, *114*, 21672.

(9) Zhang, C. J.; Hu, P. *J. Am. Chem. Soc.* **2001**, *123*, 1166.

(10) Wang, G. C.; Nakamura, J. *Journal of Physical Chemistry Letters* **2010**, *1*, 3053.

(11) Imbihl, R.; Ertl, G. *Chemical Reviews* **1995**, *95*, 697.

(12) Grunes, J.; Zhu, J.; Anderson, E. A.; Somorjai, G. A. *J. Phys. Chem. B* **2002**, *106*, 11463.

(13) Semagina, N.; Kiwi-Minsker, L. *Cat. Rev.* **2009**, *51*, 147.

(14) Tao, A. R.; Habas, S.; Yang, P. D. *Small* **2008**, *4*, 310.

(15) Xia, Y.; Xiong, Y. J.; Lim, B.; Skrabalak, S. E. *Angew. Chem., Int. Ed.* **2009**, *48*, 60.

(16) Lim, B.; Jiang, M. J.; Tao, J.; Camargo, P. H. C.; Zhu, Y. M.; Xia, Y. N. *Adv. Funct.*

Mater. **2009**, *19*, 189.

(17) Lim, B.; Xiong, Y. J.; Xia, Y. N. *Angew. Chem., Int. Ed.* **2007**, *46*, 9279.

(18) Gehl, B.; Frömsdorf, A.; Aleksandrovic, V.; Schmidt, T.; Pretorius, A.; Flege, J.-I.; Bernstorff, S.; Rosenauer, A.; Falta, J.; Weller, H.; Bäumer, M. *Adv. Funct. Mater.* **2008**, *18*, 2398.

(19) Lange, C.; De Caro, D.; Gamez, A.; Storck, S.; Bradley, J. S.; Maier, W. F. *Langmuir* **1999**, *15*, 5333.

(20) Wang, Z. L.; Petroski, J. M.; Green, T. C.; El-Sayed, M. A. *J. Phys. Chem. B* **1998**, *102*, 6145.

(21) Yu, R.; Song, H.; Zhang, X. F.; Yang, P. D. *J. Phys. Chem. B* **2005**, *109*, 6940.

(22) Lee, I.; Morales, R.; Albiter, M. A.; Zaera, F. *Proc. Natl. Acad. Sci. U. S. A.* **2008**, *105*, 15241.

(23) Vig, J. R. *J Vac Sci Technol A* **1985**, *3*, 1027.

(24) Aliaga, C.; Park, J. Y.; Yamada, Y.; Lee, H. S.; Tsung, C.-K.; Yang, P.; Somorjai, G. A. *J. Phys. Chem. C* **2009**, *113*, 6150.

(25) Pang, S.; Kurosawa, Y.; Kondo, T.; Kawai, T. *Chem. Lett.* **2005**, *34*, 544.

(26) Griffiths, P. R.; de Haseth, J. A. *Fourier Transform Infrared Spectrometry*; Wiley: New York, 1986.

(27) Andanson, J.-M.; Baiker, A. *Chem. Soc. Rev.* **2010**, *39*, 4571.

(28) Tribolet, P.; Kiwi-Minsker, L. *Catalysis Today* **2005**, *102*, 15.

(29) Siffalovic, P.; Chitu, L.; Majkova, E.; Vegso, K.; Jergel, M.; Luby, S.; Capek, I.; Satka,

A.; Maier, G. A.; Keckes, J.; Timmann, A.; Roth, S. V. *Langmuir* **2010**, *26*, 5451.

(30) Penner, S.; Di, W.; Jenewein, B.; Gabasch, H.; Klotzer, B.; Knop-Gericke, A.; Schlogl, R.; Hayek, K. *J. Chem. Phys.* **2006**, *125*.

(31) Zheng, G.; Altman, E. I. *Surf. Sci.* **2002**, *504*, 253.

(32) Lundgren, E.; Gustafson, J.; Mikkelsen, A.; Andersen, J. N.; Stierle, A.; Dosch, H.; Todorova, M.; Rogal, J.; Reuter, K.; Scheffler, M. *Phys. Rev. Lett.* **2004**, *92*.

(33) Boehm, H. P. *Carbon* **2002**, *40*, 145.

(34) Biniak, S.; Szymanski, G.; Siedlewski, J.; Swiatkowski, A. *Carbon* **1997**, *35*, 1799.

(35) Yue, Z. R.; Jiang, W.; Wang, L.; Gardner, S. D.; Pittman, C. U. *Carbon* **1999**, *37*, 1785.

(36) Borodko, Y.; Habas, S. E.; Koebel, M.; Yang, P.; Frei, H.; Somorjai, G. A. *J. Phys. Chem. B* **2006**, *110*, 23052.

(37) Szanyi, J.; Kuhn, W. K.; Goodman, D. W. *J Vac Sci Technol A* **1993**, *11*, 1969.

(38) Burgi, T. *Phys. Chem. Chem. Phys.* **2001**, *3*, 2124.

(39) Bradley, J. S.; Millar, J. M.; Hill, E. W.; Behal, S.; Chaudret, B.; Duteil, A. *Faraday Discuss.* **1991**, *92*, 255.

(40) Borodzinski, A.; Bond, G. C. *Catal. Rev.-Sci. Eng.* **2008**, *50*, 379.

(41) Teschner, D.; Vass, E.; Havecker, M.; Zafeiratos, S.; Schnorch, P.; Sauer, H.; Knop-Gericke, A.; Schloegl, R.; Chamam, M.; Wootsch, A.; Canning, A. S.; Gamman, J. J.; Jackson, S. D.; McGregor, J.; Gladden, L. F. *J. Catal.* **2006**, *242*, 26.

(42) Borodzinski, A.; Cybulski, A. *Appl. Catal., A* **2000**, *198*, 51.

(43) Toebes, M. L.; van Dillen, J. A.; de Jong, Y. P. *J. Mol. Catal. A:Chem.* **2001**, *173*, 75.

(44) Lee, H.; Habas, S. E.; Kweskin, S.; Butcher, D.; Somorjai, G. A.; Yang, P. D. *Angew. Chem., Int. Ed.* **2006**, *45*, 7824.

(45) Schroder, U.; Schoon, N. H. *J. Catal.* **1993**, *143*, 381.

(46) Cider, L.; Schoon, N. H. *Appl. Catal.* **1991**, *68*, 191.

(47) Cider, L.; Schroder, U.; Schoon, N. H.; Albinsson, B. *J. Mol. Catal.* **1991**, *67*, 323.

(48) Weiss, A. H.; Gambhir, B. S.; LaPierre, R. B.; Bell, W. K. *Industrial & Engineering Chemistry Process Design and Development* **1977**, *16*, 352.

(49) Wehrli, J. T.; Thomas, D. J.; Wainwright, M. S.; Trimm, D. L.; Cant, N. W. *Appl. Catal.* **1991**, *70*, 253.

(50) Primet, M.; El Azhar, M.; Guenin, M. *Appl. Catal.* **1990**, *58*, 241.

(51) Chen, J. Y.; McLellan, J. M.; Siekkinen, A.; Xiong, Y. J.; Li, Z. Y.; Xia, Y. N. *J. Am. Chem. Soc.* **2006**, *128*, 14776.

(52) Xiong, Y. J.; Cai, H. G.; Wiley, B. J.; Wang, J. G.; Kim, M. J.; Xia, Y. N. *J. Am. Chem. Soc.* **2007**, *129*, 3665.

(53) Rottman, C.; Wortis, M. *Phys Rev B* **1981**, *24*, 6274.

SYNOPSIS TOC GRAPHIC